Effect of Induction and Blade Elasticity Modelling on Wind Turbine Rotor Performance Predictions

Effect of Induction and Blade Elasticity Modelling on Wind Turbine Rotor Performance Predictions

Navid Aryan[1], İldeniz Öztürk[2,4], Muhammad Juanda Putra[3,4], Nilay Sezer-Uzol[2,4], Elif Oğuz[3,4], Luca Greco[5]

[1] Department of Mechanical and Aerospace Engineering (DIMA), Sapienza University of Rome, Via Eudossiana 18, 00184, Rome, Italy.
[2] Dept. of Aerospace Engineering, [3] Dept. of Civil Engineering, and [4] Center for Wind Energy Research (RÜZGEM), Middle East Technical University (METU), Ankara, Türkiye.
[5] CNR-INM - Institute of Marine Engineering, Via di Vallerano 139, 00128 Rome, Italy.

.

E-mail: ildeniz@metu.edu.tr, navid.aryan@uniroma1.it

Abstract.

This study investigates the impact of blade induction modelling on the accuracy of wind turbine rotor aeroelastic predictions. It extends the capabilities of AEOLIAN (AErOeLastic sImulAtioN), a Fluid Structure Interaction (FSI) solver based on Blade Element Momentum Theory (BEMT) coupled with a Lumped Mass approach to represent the blade structure. Herein, AEOLIAN's analytical wake induction engineering model is replaced with the outcomes of a physically-consistent three-dimensional Free-Vortex Wake (FVW) formulation initially employed in AeroROTOR. This versatile aeroelastic simulation tool is implemented within the framework of MATLAB Simulink/Simscape-Multibody©, a modular environment suitable for industry analysts, researchers, and academic users focusing on wind turbine aero-servo-elastic applications. Furthermore, it serves to lay the groundwork for the development of advanced control laws for multi-megawatt rotors, fostering innovation in the design and optimization of the next-generation wind turbines. The presented analyses focus on predicting the aeroelastic behavior of the bottom-fixed NREL 5MW rotor in uniform axial flow over the operating range, complemented by more detailed investigations at the rated condition undergoing inflow with/without wind misalignment (yaw). The study on key performance parameters is conducted by comparing with the higher-fidelity data from available Computational Fluid Dynamics (CFD) and Computational Structural Dynamics (CSD) coupled with CFD.

1. Introduction

Aeroelasticity modelling stands as a cornerstone in designing the next generation of larger and lighter-weight multi-megawatt Wind Turbine (WT) rotors, with a particular focus on diminishing the wind energy production costs. Recent research projects [1] and collaborative efforts like IEA Tasks 29 and 47 [2], underline the persistent challenge of accurately estimating blade loads and rotor responses, particularly in off-design conditions and for Floating Offshore Wind Turbines (FOWTs) applications.

The literature presents a spectrum of fully-coupled aero–servo–elastic methodologies, each varying in fidelity levels. The hierarchy of aerodynamic methodologies ranges from engineering-type Blade Element Momentum Theory (BEMT) [3], to mid-fidelity Panel Methods [4], and to high-fidelity Computational Fluid Dynamics (CFD) solvers [5]. These methodologies are coupled with blade structural models relying on the two/three-dimensional Finite Element Method (FEM) [6] or Euler-Bernoulli 1D beam modelling [7, 8]. Nevertheless, many of the tools used

for industrial applications are based on the engineering aerodynamic models (mainly BEMT), which are computationally affordable for aeroelastic computations and are built upon specific assumptions. Yet, gauging their reliability as the physical phenomena escalates in complexity, needs a case-by-case investigation.

Among the existing solvers and approaches, a synthesis of engineering and mid-fidelity methodologies facilitates a judicious enhancement, balancing simplified assumptions while still avoiding the high computational costs associated with the higher-fidelity CFD simulations.

The present work describes the development and assessment of a two-way Fluid Structure Interaction (FSI) model for the comprehensive analysis of WTs rotor aeroelasticity within the framework of MATLAB Simulink/Simscape-Multibody©. Blade structural dynamics is based on a linear beam model solved by the Lumped Mass (LM) approach implemented in FSI solver AEOLIAN (AErOeLastic sImulAtioN) [9]. The modelling capabilities of the BEMT-based aerodynamic formulation in AEOLIAN are improved by replacing its steady analytical wake induction engineering model with the outcomes of the physically-consistent three-dimensional unsteady free-vortex wake (FVW) formulation used in AeroROTOR [10] suitable for the accurate description of the vortical structure released by the blade trailing edge. This aspect becomes particularly relevant in the analysis of on- or offshore WTs in off-design conditions.

The combination of the proposed solvers is achieved by leveraging the possibilities provided by the Simulink framework, and demonstrates the versatility of such an approach. Compared to the available tools using a similar strategy [11, 12, 13], the present formulation includes blade elasticity as well as more accurate induction modelling, and, it has been implemented within an environment with versatile already-implemented features being highly adaptable for integration with other tools. Furthermore, with respect to the widely used QBlade and OpenFAST codes [14, 15], the proposed tool has the potential to facilitate the implementation of sophisticated control algorithms in MATLAB, enabling adaptive and responsive operational strategies.

Starting from this scenario, this paper focuses on the aeroelastic analysis of NREL 5MW rotor operating in uniform axial and yawed flow conditions. The evaluation of the proposed models relies on higher-fidelity reference data obtained through a CFD-CSD approach in which blade forces are computed by an incompressible Reynolds-Averaged Navier-Stokes (RANS) solver, and are coupled with the FEM solution of blade structural dynamics based on the second-order, nonlinear, isotropic, Euler-Bernoulli cantilever beam undergoing moderate deformations [16, 17].

2. Numerical Modelling

Coordinate Systems Considering a FOWT system, the following Coordinate Systems (CS) are introduced (see Fig.1): i) the platform CS has its origin at the base of the tower and coincides with the inertial frame for a bottom-fixed wind turbine; ii) the hub-fixed frame is centred at the rotor hub and is tilted with respect to the platform CS about its y axis (positive tilt, δ, refers to a nose-up rotation); iii) the hub-rotating CS has its origin at the centre of the hub and rotates about the x axis of the hub-fixed frame with the angular velocity Ω; iv) the global undeformed CS is defined from the hub-rotating CS after a rotation β about its y axis (positive β is considered to orient the blade upwind); v) the local undeformed CS is centred at the pitch center of each blade section and rotated with respect to the global undeformed CS about y (if the prebend angle is considered) and z to consider pitch (if exists) and twist angle.

The aerodynamic and structural models herein combined are briefly described in the following.

Aerodynamics: AeroROTOR is a mid-fidelity solver based on the combination of Blade Element Theory (BET) and Lifting-Line (LL) FVW model to provide aerodynamic loads, inflow and wake shape predictions for a WT rotor in different steady or unsteady operating conditions [10]. Each rotating blade is modelled as a LL placed along the span following the pitch axis, discretized into a N_b number of elements. Correspondingly, the surface of the wake is represented by a zero-thickness layer (shed and trailed from the LL) where the vorticity generated on the

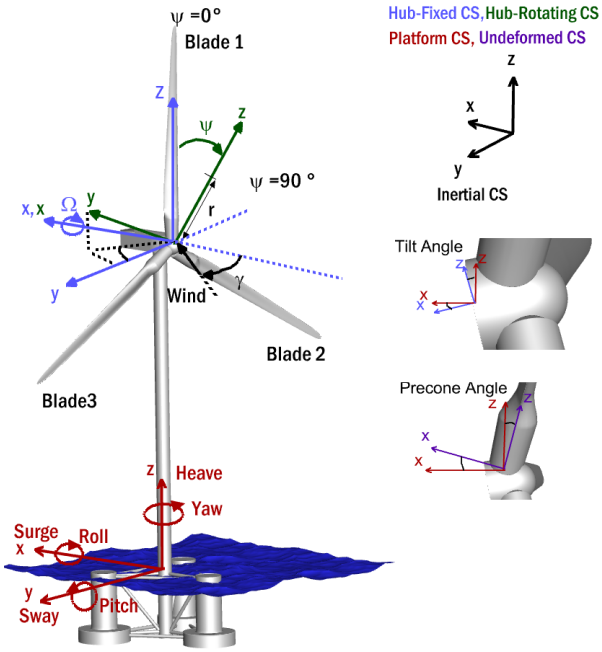

Figure 1: Definition of coordinate systems and platform degrees of freedom.

blade surface is released downstream. Numerically, this is represented by a network of vortex segments. The aerodynamic problem is solved by the following procedure: *i*) the Lifting Line theory is combined with a vortex-lattice wake to calculate the circulation strength of trailing and shed vortices. Here, the trailing vorticity accounts for the effects of spanwise circulation variation, while the shed vorticity accounts for the effects of bound vortex variation with time; *ii*) induced velocities on the LL due to the rotor wake and to the bound vortices of the other blades are calculated by using the Biot-Savart law combined with a suitable vortex core model; *iii*) the local angle of attack (AoA) and local relative flow speed are computed; *iv*) a look-up table for airfoil aerodynamic lift, drag and moment data is used and blade aeroloads are calculated using BET; *v*) blade and wake circulation is recomputed by applying the Kutta-Joukowski theorem once sectional loads are known. In FVW, the induced velocities on each wake point are combined with the incoming wind and the externally imposed motion (if any) to align the wake to the local flowfield. This procedure is iterated until a steady-periodic solution is achieved.

In the LLFVW model, the vortex core model and its value at the lifting-line (r_{core0}) are critical parameters affecting the calculation of the induced velocity field [18, 19]. Therefore, parametric analyses addressing different core models and initial core radius (r_{core0}) values are conducted. In Figs.2a and d, which depict the sensitivity analysis of predicted thrust and power with respect to the nondimensional value of r_{core0}/R (where R is the rotor radius), it is observed that LLFVW results converge towards CFD data as r_{core0} decreases, regardless of the core model. Nevertheless, the reduction of r_{core} beyond a certain value leads to numerical convergence issues of the wake alignment procedure. The effect of different vortex core models (namely Scully, Vatistas and Oseen-Lamb [18]) is also assessed in Figs. 2a and 2d. Consequently, an initial value of $r_{core0} = 0.03R$ and the Oseen-Lamb core model are used in the present analysis as a compromise between predictive accuracy and numerical stability.

Unlike BEMT, FVW methods yields a physically-consistent decrease in induced velocity at the blade tip; consequently, when coupled with BET, this approach yield an unphysical increase of lift, locally. To achieve zero-lift at the blade tip, as normally done in BEMT approaches through Prandtl correction, a combined strategy is herein applied. This involves adjusting r_{core} and applying an elliptical blade lift correction at the outboard blade sections. The impact of

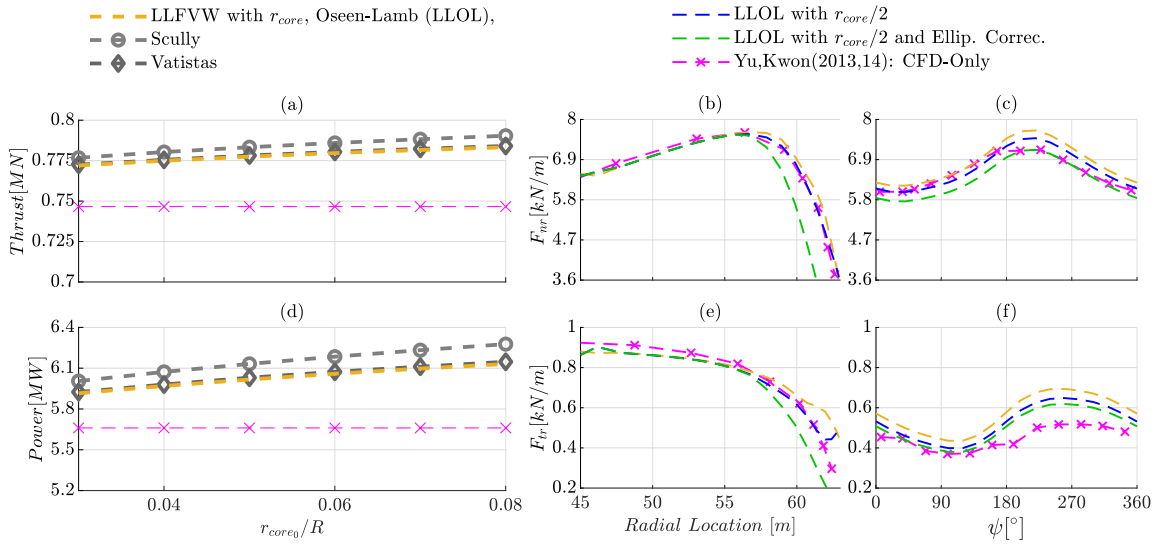

Figure 2: LLFVW solver setup: effect of vortex core model and size on thrust and power (a, d); effect of vortex core size and elliptical lift correction on blade loads in uniform (b, e) and yaw case (c, f). Reference data from [16] in axial flow and [17] for yawed flow.

such strategy, on normal (F_{nr}) and tangent-to-rotor disk (F_{tr}) forces is shown in Figs. 2b and 2e for the axial uniform flow condition and in Figs.2c and 2f for the yawed flow case. It is observed that under steady conditions, halving the value of r_{core} for the lifting line and all the wake vortex segments is sufficient to improve the accuracy of the LLFVW solver, whilst starting the elliptical correction at $r/R = 0.89$ produces an excessive underestimation of loads. Differently, in the unsteady conditions a good compromise in the prediction of F_{nr} and F_{tr} is achieved by integrating an elliptical correction initiated at $r/R = 0.91$, alongside the core reduction.

Structure: **AEOLIAN** blade structural modelling is based on the Lumped Mass (LPM) approach previously used in [9]. This method involves constructing a unified assembly, where each component is systematically built upon the one preceding it via a sequential progression facilitated by connections defining the physical relation between the components. Adding frames (i.e., conceptual axis triumvirate that contain the location and orientation data) helps using joints and constraints, apply forces and torques, and sense motion. *Frame*s and Rigid Body Transformation (*RGT*) *de facto* define the structural modelling.

A sketch of this methodology, implemented in MATLAB Simulink/Simscape-Multibody© is shown in Fig.3. Starting from the location of platform *CS*, translational and rotational *RGT*s help to get to the hub-fixed *CS* (see Fig.1). In *Blade Rotation* block, just before blades' blocks, a revolute primitive joint defines the rotational acceleration, velocity and angle about the x axis of hub-fixed *CS*. This is subsequently transformed by a rotation of β around the y axis of hub-rotating *CS* to consider the precone angle. Once more, RGT helps to reach the global undeformed *CS* (see Fig.1) at the root of the blade.

Rotor blades structure is modelled following the approach in [20], approximating flexible slender bodies as a collection of connected discrete units. Following this, the structure is discretized into several Generalized Beam Elements (GBEs: see Fig.3b) where each is a *body*-joint-*body* combination able to capture deformations that are small and linear. Every *body* is represented as a rigid mass while the structure as a whole remains flexible. In more details, each unit includes two (or more) rigid mass elements (LE, Lower Element and UE, Upper Element.), centered at blades' sections pitch center. LE and UE are interfaced by a gimbal joint providing a 3-DOF rotation through a sequence of uncoupled rotational springs and dampers ($\mathbf{R_x}$,$\mathbf{R_y}$ and $\mathbf{R_z}$). Each sequence considers the previous one as the base for the subsequent rotation resulting the final one to be obtained through R transformation ($\mathbf{R} = \mathbf{R_x}\mathbf{R_y}\mathbf{R_z}$) of its base frame. Such

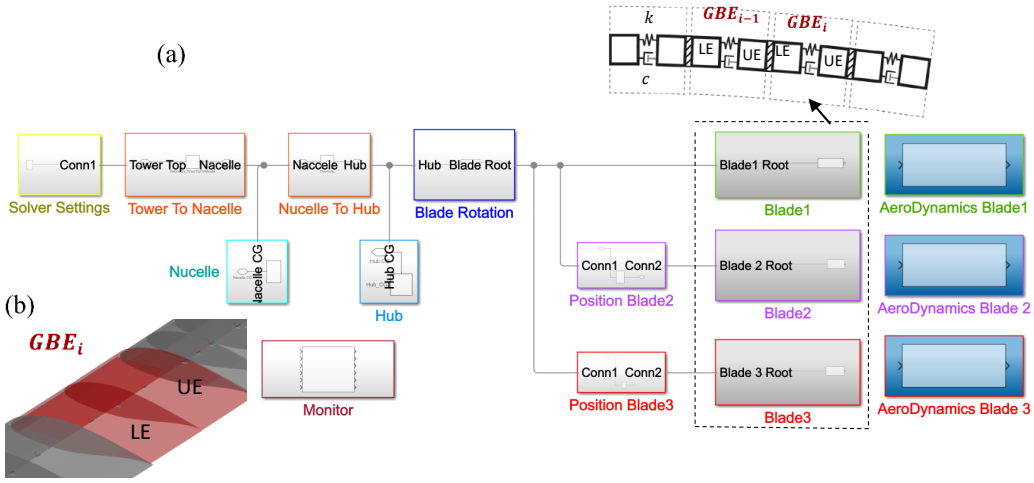

Figure 3: Sketch of blade structural modelling in AEOLIAN implemented in MATLAB Simulink/Simscape-Multibody©.

joint is used to model blades' flapwise, edgewise and torsional deformations.

Integration of tools A robustly-coupled two-way FSI procedure in the time-domain is achieved by integrating AEOLIAN structural module and AeroROTOR aerodynamic solver. During each simulation time step, the data about displacement and rotation of each blade section is transmitted from the structural solver to the aerodynamic one. Specifically, a quasi-steady approach is employed, where the impact of the deformation velocity on blade sectional aerodynamics is considered negligible. Consequently, the computation of AoA results from the rotation of each blade section due to its deformation. Then, F_{nr}, F_{tr} and pitching moment (M_θ) are calculated and exerted on the deformed blade for the computation of the solution at the next time step. This process persists until a converged behavior is achieved. The synchronization between structural and aerodynamic solutions is achieved by communicating the aerodynamic loads at prescribed azimuthal steps and keeping them constant over multiple structural time steps. The DAESSC (Differential Algabric Solver for Simscape) solver numerically integrates the corresponding aeroelastic system of equations.The intricacies associated with implementing a conventional FSI solver are reduced by heavily relying on the implementation environment to update operating points, system's state and deformed blades' locations resulting in a notable reduction of the process complexity. Furthermore, the integration of both aerodynamics and structural components within the same environment is fundamental in sidestepping the challenges typically associated with partitioned FSI approaches.

3. Results and Discussion

LLFVW-LPM method, detailed in Section 2, and BEMT-LPM [9] are applied to analyse the NREL 5 MW WT aeroelastic behaviour. Details about rotor properties can be found in [21], where airfoil characteristics (same for both solvers) are corrected for rotational stall-delay effects using the Selig and Eggars method, and then, are extrapolated up to $\pm 180°$ through the Viterna correction. Differently, no correction is applied to the pitching moment [21]. In the LLFVW model, blades are discretized using 48 elements whereas rotor revolution is divided into 10° azimuthal time steps, following the recommendation of [22]. Furthermore, the convergence analysis (omitted for brevity) shows that predicted loads become independent of wake extension if 10 revolutions are used for the computations. In the following, *CFD-Only* denotes aerodynamics computations, whereas *CFD-CSD* indicates the aeroelastic ones.

The general description of the investigated cases and reference data is reported in Table 1.

Case	V_W	RPM	Yaw	Tilt	Precone	Configuration	Reference	Section
1	11.5	12.1	×	×	✓	2-way FSI	Beam-CFD [16]	3.2
2	11.5	12.1	30°	✓	✓	2-way FSI	Beam-CFD [17]	3.3

Table 1: List of investigated cases (V_W: free-stream wind velocity; RPM: rotor speed).

3.1. Uniform Axial Flow - Over the operating range

The uniform axial flow over the operating wind speed of 4 to 20 m/s, is herein considered (11.5 m/s is the rated V_W). The rotor speed at below-rated conditions is taken from [16] whilst RPM and pitch control settings assuring the nominal rotor power at above-rated condition are summarized in Table 2. The effect of the gravitational force and shaft tilt are neglected to comply with the higher-fidelity reference data used for codes-to-code comparison [16].

V_W	**Rotor Speed**	**Pitch Setting** [°]		
$[m/s]$	All Models $[RPM]$	LLFVW	BEMT [9]	CFD-CSD [16]
11.5	12.1	0	0	0
15	12.1	8.8	8.6	8.4
20	12.1	15.9	15.7	15.3

Table 2: NREL 5 MW - Uniform axial flow: control settings at rated and above-rated wind speeds. Reference data from [16].

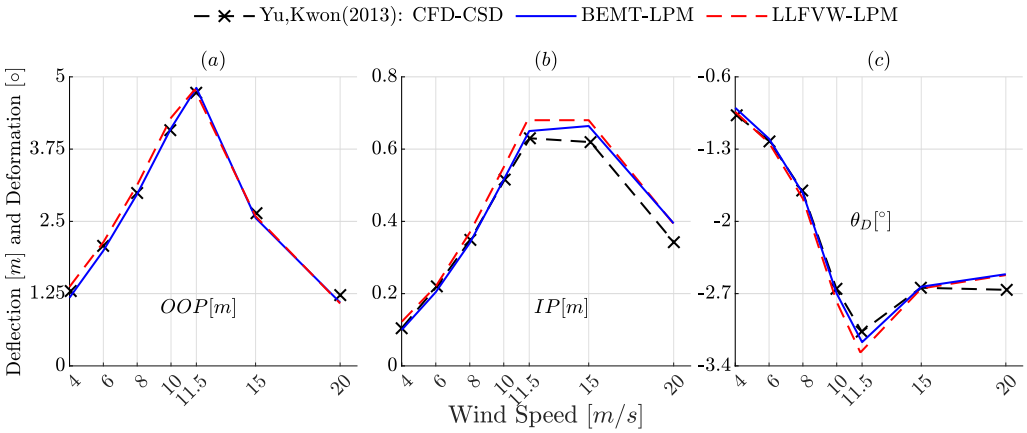

Figure 4: NREL 5 MW - Uniform axial flow: blade tip deflection (a, b) and torsional deformation (c) compared to CFD-CSD data from [16].

Figure 4 shows the in-plane (IP), out-of-plane (OOP) and torsional (θ_D, positive nose-up) blade deformation. It is observed that OOP and IP deflection predictions by BEMT and LLFVW are in good agreement as against the reference data with an average error below 5%. Slightly higher discrepancy on IP is exhibited at above-rated conditions, where small changes in blade pitch setting (and torsional deformation) can significantly impact blade loads. Regarding the blade torsional deformation (θ_D), as can be seen in Figure 4c, the maximum error of 3% and 6% is observed for BEMT and LLFVW respectively, at the rated condition (see Section 3.2).

Table 3 summarizes the predicted rotor torque and thrust. A maximum error of 14% on torque estimation by BEMT and 3% for LLFVW is observed. Similarly, the largest discrepancy on thrust is 9% for BEMT and $< 3\%$ for LLFVW. Above the rated wind speed, torque accuracy is maintained within 4% for LLFVW and 1.5% for BEMT, whilst the maximum deviation in thrust is higher for BEMT (approximately 3.5%) than LLFVW (1.5%), both remaining in good agreement with the reference data.

As a general comment, the use of a more sophisticated induction model (*i.e.*, the LLFVW) yields a significant improvement of rotor loads predictions over the operating range, especially below the rated wind speed. Differently, no notable variance is observed for blade deflections.

V_W	**Torque** $[MNm]$			**Thrust** $[MN]$		
$[m/s]$	LLFVW	BEMT	CFD-CSD	LLFVW	BEMT	CFD-CSD
4	0.39	0.24	0.28	0.14	0.12	0.13
6	1.09	0.94	1.10	0.24	0.22	0.24
8	2.09	1.90	2.08	0.38	0.35	0.37
10	3.19	2.94	3.10	0.56	0.52	0.55
11.5	4.30	4.20	4.26	0.68	0.72	0.67
15	4.39	4.20	4.21	0.45	0.33	0.44
20	4.39	4.17	4.26	0.34	0.28	0.30

Table 3: NREL 5 MW - Uniform axial flow: rotor torque and thrust predictions over the operating range. Reference data from [16].

3.2. Case I: Uniform Axial Flow - Rated wind speed

A more detailed analysis of the rated condition is herein addressed (Case 1 in Table 1). The reference data is the same as in Section 3.1. The outcomes are illustrated in Fig.5 for both the rigid and deformable blade configurations.

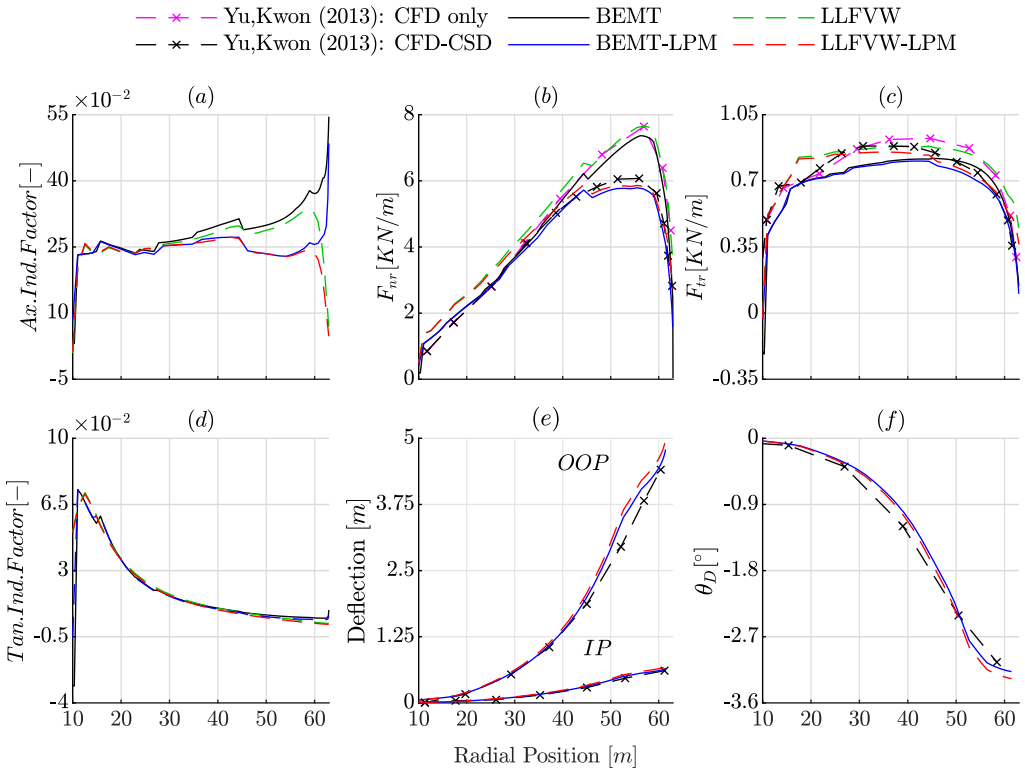

Figure 5: NREL 5 MW rotor - Spanwise distribution of (a) a, (b) F_{nr}, (c) F_{tr} (d) a' (e) OOP and IP (f) θ_D. Reference data from Yu-Kwon (2013)[16]

A consistent trend is observed, with the higher-fidelity model generally predicting lower axial induction factor (a) close to the tip (see Fig.5a). This different behaviour is due to the use of Prandtl tip correction in BEMT, while the tip loss is inherently incorporated into the 3D solution of the FVW model. The effect of blade elasticity on the tangential induction factor (Fig.5d) is minimal, with LLFVW and BEMT exhibiting coincident predictions. The analysis of the spanwise distribution of blade forces (F_{nr} and F_{tr}), depicted in Fig.5b and c, indicates that both solvers capture the magnitude of loads reduction due to the presence of the blade's torsional deformation. Indeed, for a section located at $0.93R$, both models show approximately a reduction of 40% and 29% for AoA and a respectively. Correspondingly, 23% reduction in F_{nr}, 11% in F_{tr} and 6% for the pitching moment M_θ is estimated (this analysis is not shown here).

In terms of prediction accuracy, Figs.5b and c generally indicate an improvement of LLFVW predictions with respect to BEMT (see Table 4 for the quantification of the error). Nevertheless, overprediction at inboard sections from 30 m to the root is ascribable to the absence of nacelle modelling in the LLFVW model and, eventually, to local flow separation not properly captured by either induction models.

The analysis of spanwise blade deformation (Fig.5e and f) shows that OOP and IP deflections are similarly predicted by BEMT and LLFVW. An OOP of 4.8 m for BEMT and 5.01 m for LLFVW at the tip, giving an error of 9% and 13.5% , respectively, is exhibited. Similarly, the estimation of θ_D aligns well with the reference data (3.07°), where LLFVW and BEMT predict nose-down deformations of 3.27 and 3.17° respectively.

A summary of blade loads deviation from the reference data in axial flow ($\gamma = 0°$) at the rated wind speed is outlined in Table 4. In the absence of reference data for M_θ, the deviation of aeroloads predictions in the rigid blade case (superscript R) remains below 6.2% for BEMT whilst LLFVW shows better agreement remaining less than 1.5%. The error of aeroelastic predictions (superscript E), remains below 5% and 4% for BEMT and LLFVW, respectively whilst a larger deviation (approximately 10%) is observed in LLFVW predictions of F_{tr}.

3.3. Case II: Yawed flow - Rated wind speed

The yawed flow condition at $\gamma = 30°$ is herein examined (Case 2 in Table 1). The rotor tilt angle of 5° and the gravitational force are considered in order to compare present predictions with the higher-fidelity outcomes of [17]. The static Pitt and Peters [23] model is added to the BEMT formulation since a preliminary analysis (not shown here) confirmed that it yields better reconstruction of the induction factor over the azimuth.

For a blade section located at $0.93R$, Fig.6 depicts a summary of the performed analysis. As a general observation, due to the presence of yaw, aerodynamic loads and blade deflections are affected by the tangential wind component (*i.e.*, along y axis of the local undeformed *CS*, see Section 2) which is responsible for the unsteady fluctuation of these quantities over the azimuth. Furthermore, the smaller axial component of velocity due to the precone angle is responsible for lowering the mean value of aeroloads with respect to the axial flow condition at the same V_W.

In the rigid blade configuration, approximately 1.8° of *AoA* variation is experienced over the azimuth, consistently predicted by both approaches (omitted for brevity). This is reflected in the corresponding variation of F_{nr}, F_{tr} and M_θ as illustrated in Fig.6a, b and c respectively. The deviation of azimuthally-averaged load values with respect to the reference data is given in Table 4 (superscript R). As a general comment, the accuracy of normal force predictions under yaw conditions experiences a decrease of 2.6% for LLFVW in comparison to axial flow conditions. However, both models exhibit strong alignment with the reference data with deviations staying under 4.2% (BEMT) and 3% (LLFVW). A significant degradation of predictions is observed for F_{tr} where the error stands at 13.35% for BEMT and 14.56% for LLFVW. This is in line with the findings of IEA Wind Task 29 [2, 24] demonstrating the potential enhancement of solvers reliant on airfoil polar data through the utilization of lift and drag characteristics derived from CFD simulations of the same rotor.

Figures 6d to i summarize the present outcomes for the deformable blade configuration. Similarly to the axial flow case, the introduction of elasticity has the effect of decreasing the *AoA* due to blade torsional deformation. Consequently, the computed blade loads, as illustrated in Figs.6d to f for F_{nr}, F_{tr}, and M_θ respectively, are reduced with respect to the rigid case. It is observed that using the LLFVW slightly improves the predictions of F_{nr} at $0° < \psi < 180°$, whilst similar deviations with respect to CFD-CSD data are observed elsewhere. Differently, LLFVW and BEMT-based M_θ predictions show a similar level of accuracy. Finally, the dramatic reduction of F_{tr} shown by the higher-fidelity simulations (about 100% with respect to the rigid configuration) is not captured by either codes. Although this is in line with the outcomes of

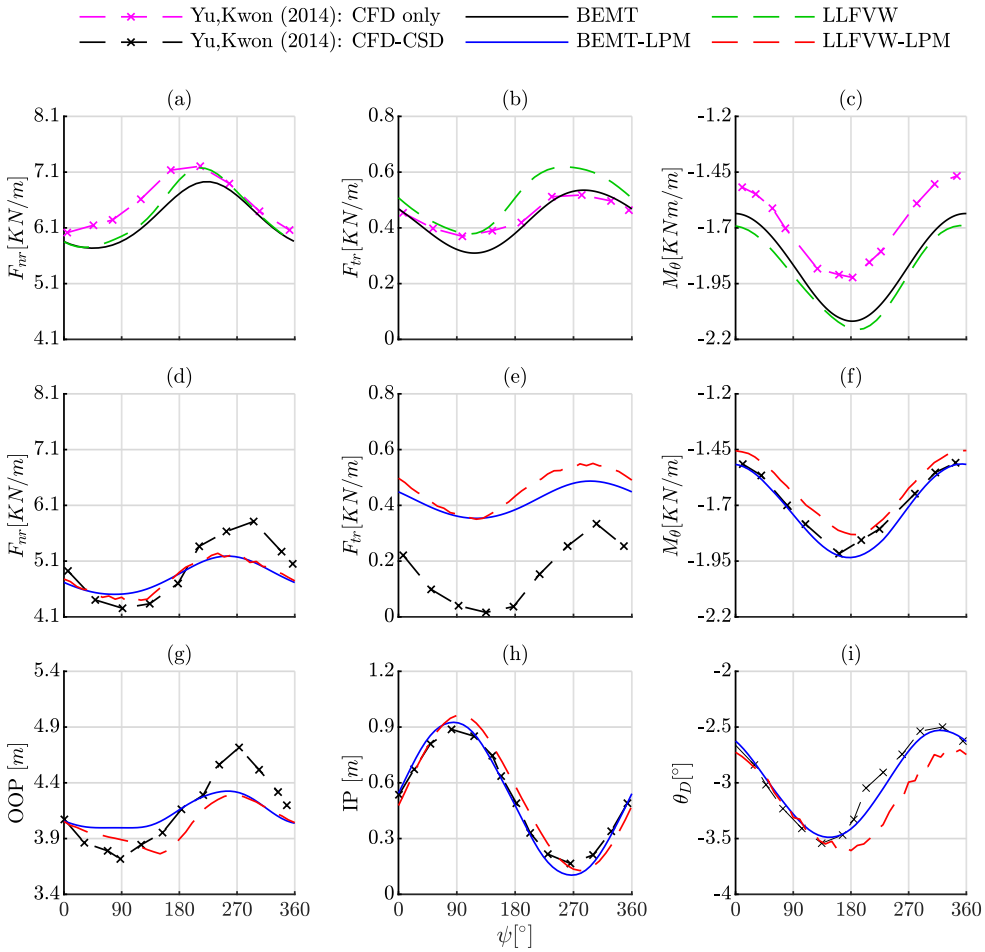

Figure 6: NREL 5 MW, Case 2: Loads and deflection analysis for a section located at $0.93R$ at $\gamma = 30°$. (a,d) F_{nr}, (b,e) F_{tr} (c,f) M_θ, (g) OOP, (h) IP, (i) θ_D. Reference data from [17].

the IEA Wind Tasks 29 and 47 [24, 2] to some extent, this level of discrepancy is higher than expected and requires further investigation.

Table 4 lists the error on the averaged blade loads for $\gamma = 30°$ (superscript E). The comparative analysis reveals a deviation of about 3% for F_{nr} and $< 4\%$ for M_θ comparing with the benchmark data, whilst the discrepancy in F_{tr} reaches 110%.

Figure 6g and h depict the azimuthal variation of OOP and IP deflection. Compared to the observation in Case 1, the average magnitude of OOP (approximately 4.8 m) is reduced due to the lower blade loading. While LLFVW predictions exhibit a marginally closer adherence to CFD-CSD trend, the overall accuracy remains comparable to BEMT computations, with a maximum error of 10% (see Fig.6g). Nonetheless, both solvers provide reasonable predictions for the azimuthally-averaged OOP deflection. Further investigation on IP (not shown here) verified that gravity governs its amplitude variation over the azimuth. Both LLFVW and BEMT shows an excellent agreement with the reference data (Fig.6h). Finally, Fig.6i illustrates the azimuthal variation of θ_D indicating a reasonable agreement between the prediction of the proposed tools with respect to the reference values (maximum deviation belongs to LLFVW with 11% as opposed to BEMT with 4%).

As a general comment, in the yawed flow case, the introduction of a more sophisticated induction modelling improves model accuracy for the rigid blade configuration whilst yielding no significant enhancement for the deformable one, although F_{nr} shows better agreement with the CFD-CSD data at specific azimuth values. The discrepancy in F_{tr} computations appears to

Code	γ°	F_{nr}^R	F_{tr}^R	M_θ^R	F_{nr}^E	F_{tr}^E	M_θ^E
BEMT	0	4.43	6.12	-	4.77	0.15	-
LLFVW	0	0.4	1.37	-	3.46	10	-
BEMT	30	4.2	13.35	10	3	110	< 1
LLFVW	30	3	14.56	13	3.3	110	4

Table 4: Mean-value error at $\gamma = 30^\circ$ with respect to [17] and at $\gamma = 0^\circ$ compared with [16] for a section located at 0.93 of blade length (R: Rigid, E: Elastic).

be a key contributor to the overall deviation from CFD-CSD data.

4. Conclusions

The aeroelastic analysis of the bottom-fixed NREL 5MW rotor employing two diverse methods of induction modelling - specifically BEMT and LLFVW - coupled in a two-way approach with a LPM multibody-based formulation of blades' structural dynamics is herein investigated. Both solvers are implemented within MATLAB Simulink/Simscape-Multibody© framework.
Drawing a comparison to the higher-fidelity CFD-CSD model, computations illustrate that:

- in axial flow conditions over the operating range, the improved induction modelling from LLFVW, results in significantly better rotor loads predictions below the rated wind speed and similar accuracy above it. Nevertheless, no notable variance is observed for blade deflections indicating similar performance between both models;
- considering the rated condition, at a section located at $0.93R$, a 40% reduction of AoA with respect to the rigid blade configuration is predicted by both models. Consequently, 23% reduction in F_{nr}, 11% in F_{tr} and a slightly less value (6%) for M_θ is observed;
- in yawed flow conditions, the use of LLFVW approach generally improves blade force azimuthal predictions in the rigid blade configuration, whilst no significant impact is observed for blade loads and deformations in the aeroelastic computations, as both solvers exhibit similar levels of accuracy;
- the observed excessive overestimation of F_{tr} in the elastic yawed flow case needs further investigation.

References

[1] FLOATECH `https://www.floatech-project.com/`
[2] Boorsman K *et al.* 2023 *Wind Energy*
[3] Ning *et al.* 2015 *33rd Wind Energy Symposium*
[4] Greco L and Testa C 2021 *Renewable Energy*
[5] Schulz *et al.* 2017 *Wind Energy*
[6] Bazilevs *et al.* 2011 *Int. J. Numer. Methods Fluids*
[7] Jonkman *et al.* 2005 *FAST user's guide* (NREL, CO, USA)
[8] Larsen *et al.* 2007 *How 2 HAWC2, the user's manual* (Risø National Laboratory)
[9] Aryan N, Greco L and Testa C 2023 *OSES23 Conference Proceedings*
[10] Öztürk I and Sezer-Uzol N 2023 *OSES23 Conference Proceedings*
[11] Sirigu M *et al.* 2022 *J. Phys.: Conf. Ser.*
[12] Ning S 2013 Ccblade documentation: Release 0.1. 0
[13] Shaler K, Branlard E and Platt A 2020 Olaf user's guide and theory manual
[14] Marten D, Wendler J, Pechlivanoglou G, Nayeri C N and Paschereit C O 2013 *IJETAE*
[15] Jonkman J M *et al.* 2015 *AeroDyn v15 user's guide and theory manual*
[16] Yu D and Kwon O 2013 *51st AIAA Aerospace Sciences Meeting*
[17] Yu D and Kwon O 2014 *Journal of Physics: Conference Series*
[18] Leishman J 2006 *Principles of Helicopter Aerodynamics* 2nd ed
[19] Sant T, van Kuik G and Van Bussel G 2006 *Wind Energy*
[20] Miller S 2017 Modeling flexible bodies with simscape multibody software
[21] Jonkman J, Butterfield S, Musial W and Scott G 2009 *Technical Report: NREL/TP-500-38060*
[22] Bhagwat M and Leishman J 2001 *39th Aerospace Sciences Meeting and Exhibit*
[23] Chen R T 1989 A survey of nonuniform inflow models for rotorcraft flight dynamics and control applications
[24] Schepers J *et al.* 2021 IEA Wind TCP Task 29, Phase IV: Detailed Aerodynamics of Wind Turbines